Phase-Selective Synthesis of Copper Sulfide Nanocrystals

Wen Pei Lim,[†,‡] Chiong Teck Wong,[†] Si Ling Ang,[†] Hong Yee Low,[‡] and Wee Shong Chin*[,†]

Department of Chemistry, National University of Singapore, 3 Science Drive 3, Singapore 117543, and Institute of Materials Research and Engineering, 3 Research Link, Singapore 117602

Received July 20, 2006. Revised Manuscript Received October 4, 2006

Monodispersed copper sulfide nanocrystals were synthesized via the decomposition of an air-stable precursor, copper (I) thiobenzoate (CuTB), in the presence of dodecanethiol (DDT). We discover that, by varying the stabilizing agent used (trioctylphosphine or tributylphosphite), we can selectively generate phase-pure roxbyite nanoplates ($Cu_{1.75}S$) or chalcocite faceted nanocrystals (Cu_2S). We also demonstrate that, under suitable conditions, the roxbyite nanoplates can be forced to grow only in two dimensions, with an aspect ratio (diameter/thickness) tunable between 2.3 and 4.1. To the best of our knowledge, this is the first report for making nanocrystalline copper sulfide with such aspect ratio tunability. Temperature and the [DDT]/[CuTB] ratio were identified to be the important factors for controlling the size of the nanocrystals. To gain more insight to the mechanisms of phase-selective control, we attempted a series of controlled experiments and DFT calculations. It appears that the precursor can undergo two competitive pathways, leading to seeds, and thus the growth, of different crystal phases. This work thus demonstrates a general approach to phase-selective nanocrystals engineering whereby the kinetics of decomposition of a chosen precursor is readily manipulated using activating or stabilizing agents.

Introduction

Although semiconductor nanocrystals can be obtained in various sizes and geometries,[1] the shape-controlled synthesis of low-dimension nanocrystals warrants special attention because anisotropy in quantum confinement potentials can be used to produce unusual optical, magnetic, and electronic properties.[2] For example, Au or Ag nanorods exhibit anisotropic optical properties that are directly related to their aspect ratio,[3] and in the same way, CdSe luminescence[4] and Co/Fe magnetic properties[5] are affected markedly by their shape. The strong relationship between the physical properties and the shape anisotropy of the nanocrystals is foreseen to be important in the design and application of novel nanodevices.

Copper sulfide (Cu_xS, $x = 1-2$) is well-known to form a wide variety of non-stoichiometric and mixed phases, of which at least five are known to be stable at room temperature: covellite (CuS) in the "sulfur-rich region"; and anilite ($Cu_{1.75}S$), digenite ($Cu_{1.8}S$), djurleite ($Cu_{1.95}S$), and chalcocite (Cu_2S) in the "copper-rich region".[6] Cu_xS compounds in different stoichiometries have a wide range of well-established and prospective applications, for example, as p-type semiconductors,[7] solar cells,[8] superionic materials,[9] and in many chemical sensing applications.[10] Because of their unique optical and electrical properties, they are also widely applied as thin films[7,11] and composite materials.[8,12] Recently,

* Corresponding author. Telephone: 65-6516-8031. Fax: 65-6779-1691. E-mail: chmcws@nus.edu.sg.

† National University of Singapore.

‡ Institute of Materials Research and Engineering.

(1) (a) Lim, W. P.; Zhang, Z.; Low, H. Y.; Chin, W. S. *Angew. Chem., Int. Ed.* **2004**, *43*, 5685. (b) Gu, H.; Zheng, R.; Zhang, X. X.; Xu, B. *J. Am. Chem. Soc.* **2004**, *126*, 5664. (c) Lee, S. M.; Cho, S. N.; Cheon, J. *Adv. Mater.* **2003**, *15*, 441. (d) Yu, W. W.; Wang, Y. A.; Peng, X. *Chem. Mater.* **2003**, *15*, 4300. (e) Joo, J.; Na, H. B.; Yu, T.; Yu, J. H.; Kim, Y. W.; Wu, F.; Zhang, J. Z.; Hyeon, T. *J. Am. Chem. Soc.* **2003**, *125*, 11100. (f) Jun, Y. W.; Jung, Y. Y.; Cheon, J. *J. Am. Chem. Soc.* **2002**, *124*, 615. (g) Peng, Z. A.; Peng, X. *J. Am. Chem. Soc.* **2002**, *124*, 3343. (h) Manna, L.; Scher, E. C.; Alivisatos, A. P. *J. Am. Chem. Soc.* **2000**, *122*, 12700.

(2) (a) Kim, F.; Connor, S.; Song, H.; Kuykendall, T.; Yang, P. *Angew. Chem., Int. Ed.* **2004**, *43*, 3673. (b) Chen, S.; Carroll, D. L. *J. Phys. Chem. B* **2004**, *108*, 5500. (c) Maillard, M.; Giorgio, S.; Pileni, M. P. *J. Phys. Chem. B* **2003**, *107*, 2466. (d) Peng, X.; Manna, L.; Yang, W.; Wickham, J.; Scher, E.; Kadavanich, A.; Alivisatos, A. P. *Nature* **2000**, *404*, 59. (e) Hu, J.; Odom, T. W.; Lieber, C. M. *Acc. Chem. Res.* **1999**, *32*, 435.

(3) (a) Gao, J.; Bender, C. M.; Murphy, C. J. *Langmuir* **2003**, *19*, 9065. (b) El-Sayed, M. A. *Acc. Chem. Res.* **2001**, *34*, 257.

(4) (a) Li, L.; Walda, J.; Manna, L.; Alivisatos, A. P. *Nano Lett.* **2002**, *2*, 557. (b) Huynh, W. U.; Dittmer, J. J.; Alivisatos, A. P. *Science* **2002**, *295*, 2425. (c) Hu, J.; Li, L.; Yang, W.; Manna, L.; Wang, L.; Alivisatos, A. P. *Science* **2001**, *292*, 2060. (d) Li, L.; Hu, J.; Yang, W.; Alivisatos, A. P. *Nano Lett.* **2001**, *1*, 349.

(5) (a) Puntes, V. F.; Krishnan, K. M.; Alivisatos, A. P. *Science* **2001**, *291*, 2115. (b) Park, S. J.; Kim, S.; Lee, S.; Khim, Z. G.; Char, K.; Hyeon, T. *J. Am. Chem. Soc.* **2000**, *122*, 8581.

(6) Koch, D. F. A.; McIntyre, R. J. *J. Electroanal. Chem.* **1976**, *71*, 285.

(7) (a) Johansson, J.; Kostamo, J.; Karppinen, M.; Niinisto, L. *J. Mater. Chem.* **2002**, *12*, 1022. (b) Córdova, R.; Gómez, H.; Schrebler, R.; Cury, P.; Orellana, M.; Grez, P.; Leinen, D.; Ramos-Barrado, J. R.; Río, R. D. *Langmuir* **2002**, *18*, 8647. (c) Sartale, S. D.; Lockhande, C. D. *Mater. Chem. Phys.* **2000**, *65*, 63. (d) Leong, J. Y.; Yee, J. H. *Appl. Phys. Lett.* **1979**, *35*, 601.

(8) (a) Al-Dhafiri, A. M.; Russell, G. J.; Woods, J. *Semicond. Sci. Technol.* **1992**, *7*, 1052. (b) Rastogi, A. C.; Salkalachen, S. *J. Appl. Phys.* **1985**, *58*, 4442. (c) Nataren, F. Z.; Bouchikhi, B.; Chandrasekhar, S.; Crest, J. P.; Martinuzzi, P. *J. Cryst. Growth* **1982**, *59*, 409.

(9) (a) Balapanov, M. K.; Gafurov, I. G.; Mukhamed'yanov, U. K.; Yakshibaev, R. A.; Ishembetor, R. Kh. *Phys. Status Solidi B* **2004**, *241*, 114. (b) Wakamura, K.; *Solid Sate Ionics* **2002**, *149*, 73. (c) Wakamura, K.; *Phys. Rev. B* **1997**, *56*, 11593.

(10) (a) Šetkus, A.; Galdikas, A.; Mironas, A.; Šimkiene, I.; Ancutiene, I.; Janickis, V.; Kačiulis, S.; Mattogno, G.; Ingo, G. M. *Thin Solid Films* **2001**, *391*, 275. (b) Janata, J.; Josowicz, M.; DeVaney, D. M. *Anal. Chem.* **1994**, *66*, 207R.

(11) (a) Mane, R. S.; Lokhande, C. D. *Mater. Chem. Phys.* **2000**, *65*, 1. (b) Elliot, D. J.; Furlong, D. N.; Grieser, F. *Colloids Surf., A* **1998**, *141*, 9.

10.1021/cm061686i CCC: $33.50
Published on Web 12/19/2006

Cu_xS was demonstrated as a potential nanometer-scale switch.[13]

Different methods to prepare Cu_xS nanoparticles, in the form of aqueous,[14] nonaqueous,[15] microemulsion,[16] sol−gel,[17] thin films,[7,11] and polymer composites,[12,14c] have been reported. Zhao et al. reported the formation of Cu_xS nanoparticles at low temperature (90−110 °C, 40 h) via an amine-assisted hydrothermal process[18] and Gao et al. demonstrated the formation of CuS flakes and Cu_2S disks using hydrothermal microemulsions (130 °C, 15 h).[16a] The size distribution of the particles in these two hydrothermal approaches is large, and the reaction time is very long. Molecular precursors have also been used to prepare Cu_xS. Inoue et al. obtained amorphous CuS with $[Cu(en)_2]^{2+}$ and thiourea,[19] whereas a mixture of different Cu_xS phases was obtained by Parkin et al. via a low-temperature reaction of Cu(s) and S(s) in liquid ammonia.[20] Xie et al. demonstrated the preparation of phase-pure Cu_xS nanocrystals with $[Cu(NH_3)_4]^{2+}$ and thiourea, but the size distribution was large.[21] Recently, Korgel et al. reported a simple approach for preparing nearly monodisperse chalcocite Cu_2S nanodisks by the solventless thermolysis of a copper alkylthiolate molecular precursor.[22] However, the yield is relatively low (10−20%), and reaction time is fairly long (140 min for 148 °C).

Here, we report a simple method for forming monodispersed nanocrystals of phase-pure roxbyite $Cu_{1.75}S$ nanoplates and faceted chalcocite Cu_2S nanocrystals. A remarkable finding is that phase control between the chalcocite and roxbyite structure can be achieved by a simple manipulation of the kinetics of the precursor. The control of the size, shape, and aspect ratio of the nanocrystals will be demonstrated, whereas the underlying factors that determine the morphology and crystal structure of the Cu_xS nanocrystals will be elucidated. We have also attempted to gain some insight into the decomposition mechanism of the precursor by performing modeled theoretical calculations.

Experimental Section

Materials and Synthesis. All starting materials were purchased from commercial sources and used without further purification. The copper (I) thiobenzoate (CuTB) precursor was first prepared according to the literature method.[23] All procedures for the preparation of copper sulfide nanoplates and faceted nanocrystals were carried out using standard techniques under a nitrogen atmosphere. Dodecanethiol (DDT) was carefully degassed before use. For the preparation of nanoplates, a degassed solution of CuTB (0.04 g) in trioctylphosphine (TOP; 0.3 mL) was injected into a hot solution (135/160/180/210 °C) of DDT. With good mixing, the orange solution rapidly changed to brown. After 15 min, the reaction mixture was cooled to room temperature; toluene (ca. 1 mL) was then added, and the product was precipitated with ethanol. The precipitate was centrifuged, washed thoroughly with ethanol, and dried in a vacuum overnight.

Faceted nanocrystals were prepared using a similar procedure except that tributylphosphite (TBPT) was used instead of TOP. A degassed solution of CuTB (0.04 g) in tributylphosphite (TBPT; 0.2 mL) was injected into a hot solution (135/160/180 °C) of DDT. After 20 min, the reaction mixture was cooled to room temperature, and toluene was then added. The precipitate was centrifuged and dried in a vacuum overnight. No size sorting was performed for any of the samples. In the experiment, the reaction temperature and the DDT concentration were varied. The molar ratio between CuTB and DDT (denoted as [DDT]/[CuTB]) was kept between 30 and 50. Control experiments using different surfactants (oleylamine) were carried out using the same procedure.

Characterization. The powder X-ray diffraction (XRD) pattern was acquired using a Bruker GADDS D8 with Cu K radiation (λ = 0.151478 nm). Transmission electron microscopy (TEM) was performed on a Philips CM100 microscope operating at 100 kV, and high-resolution transmission electron microscopy (HRTEM) was performed on a Philips CM300 FEG instrument with an acceleration voltage of 300 kV. One drop of the nanocrystals dispersed in toluene solution was placed on a 200 mesh carbon-coated copper grid, and the grid was dried in a vacuum before analysis. The scanning electron microscopy (SEM) images were obtained by using a JEOL JSM6700 microscope, operating at 10 amp and 15 kV. The sample was coated with gold to improve contrast. Thermogravimetric analysis (TGA) was conducted on a SDT 2960 simultaneous DTA-TGA under a nitrogen atmosphere.

Computational Methodology. Density functional theory (DFT) calculations were performed using the hybrid density functional B3LYP[24] method with the effective core potential LanL2DZ basis set.[25] All reported energies in this work include zero-point energy corrections. All calculations were performed using the Gaussian 98[26] suite of programs. Optimization was performed without any constrains, and the optimized structures were verified to be equilibrium structures or transition states from frequency calcula-

(12) (a) Godovsky, D. Y.; Varfolomeev, A. E.; Zaretsky, D. F.; Chandrakanthi, R. L. N.; Kündig, A.; Weder, C.; Caseri, W. *J. Mater. Chem.* **2001**, *11*, 2465. (b) Xiong, H.; Cheng, M.; Zhou, Z.; Zhang, X.; Shen, J. *Adv. Mater.* **1998**, *10*, 529. (c) Yamamoto, T.; Kubota, E.; Taniguchi, A.; Dev, S.; Tanaka, K.; Osakada, K.; Sumita, M. *Chem. Mater*. **1992**, *4*, 570.
(13) Sakamoto, T.; Sunamura, H.; Kawaura, H.; Hasegawa, T.; Nakayama, T.; Aono, M. *Appl. Phys. Lett.* **2003**, *82*, 3032.
(14) (a) Kore, R. H.; Kulkarni, J. S.; Haram, S. K. *Chem. Mater*. **2001**, *13*, 1789. (b) Sugimoto, T.; Chen, S.; Muramatsu, A. *Colloids Surf., A* **1998**, *135*, 207. (c) Yumashev, K. V.; Prokoshin, P. V.; Malyarevich, A. M.; Mikhailov, V. P.; Artemyer, M. V.; Gurine, V. S. *Appl. Phys. B* **1997**, *64*, 73. (d) Silvester, E. J.; Grieser, F.; Sexton, B. A.; Healy, T. W. *Langmuir* **1991**, *7*, 2917.
(15) (a) Wan, S.; Guo, F.; Peng, Y.; Shi, L.; Qian, Y. *Chem. Lett.* **2004**, *33*, 1068. (b) Osakada, K.; Taniguchi, A.; Kubota, E.; Dev, S.; Tanaka, K.; Kubota, K.; Yamamoto, T. *Chem. Mater*. **1992**, *4*, 562.
(16) (a) Zhang, P.; Gao, L. *J. Mater. Chem.* **2003**, *13*, 2007. (b) Dixit, S. G.; Mahadeshwar, A. R.; Haram, S. K. *Colloids Surf., A* **1998**, *133*, 69. (c) Haram, S. K.; Mahadeshwar, A. R.; Dixit, S. G. *J. Phys. Chem.* **1996**, *100*, 5868.
(17) (a) Gurin, V. S.; Alexeenko, A. A.; Prakapenka, V. B.; Kovalenko, D. L.; Yumashev, K. V.; Prokoshin, P. V. *Mater. Sci.* **2002**, *20*, 29. (b) Malyarevich, A. M.; Yumashev, K. V.; Posnov, N. N.; Mikhailov, V. P.; Gurin, V. S.; Prokopenko, V. B.; Alexeenko, A. A.; Melnichenko, I. M. *J. Appl. Phys.* **2000**, *87*, 212.
(18) Lu, Q.; Gao, F.; Zhao, D. *Nano Lett.* **2002**, *2*, 725.
(19) Grijalva, H.; Inoue, M.; Boggavarapu, S.; Calvert, P. *J. Mater. Chem.* **1996**, *6*, 1157.
(20) Henshaw, G.; Parkin, I. P.; Shaw, G. A. *J. Chem. Soc., Dalton Trans.* **1997**, 231.
(21) Jiang, X.; Xie, Y.; Lu, J.; He, W.; Zhu, L.; Qian, Y. *J. Mater. Chem.* **2000**, *10*, 2193.
(22) (a) Sigman, M. B.; Ghezelbash, A.; Hanrath, T.; Saunders, A. E.; Lee, F.; Korgel, B. A. *J. Am. Chem. Soc.* **2003**, *125*, 16050. (b) Larsen, T. H.; Sigman, M. B.; Ghezelbash, A.; Doty, R. C.; Korgel, B. A. *J. Am. Chem. Soc.* **2003**, *125*, 5638.
(23) Savant, V. V.; Gopalakrishnan, J.; Patel, C. C.; *Inorg. Chem.* **1970**, *9*, 748.
(24) (a) Lee, C.; Yang, W.; Parr, R. G. *Phys. Rev. B* **1988**, *37*, 785. (b) Becke, A. D. *J. Chem. Phys.* **1993**, *98*, 5648.
(25) (a) Dunning, T. H., Jr.; Hay, P. J. In *Modern Theoretical Chemistry*; Schaefer, H. F., III, Ed.; Plenum: New York, 1976; pp 1−28. (b) Hay, P. J.; Wadt, W. R. *J. Chem. Phys.* **1985**, *82*, 270. (c) Wadt, W. R.; Hay, P. J. *J. Chem. Phys.* **1985**, *82*, 284. (d) Hay, P. J.; Wadt, W. R. *J. Chem. Phys.* **1985**, *82*, 299.

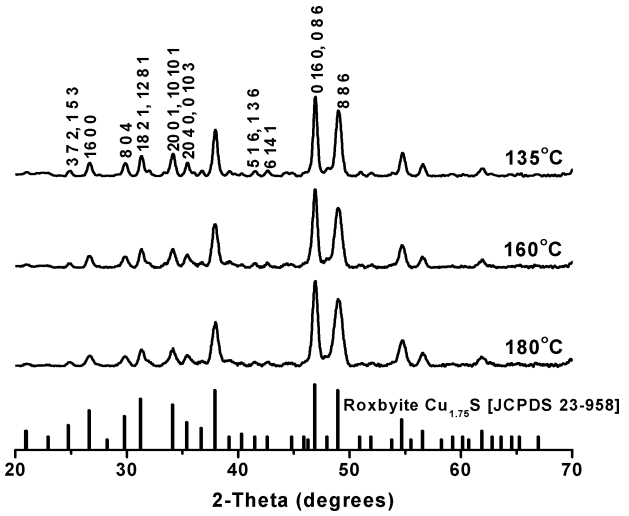

Figure 1. Representative XRD patterns of the $Cu_{1.75}S$ nanoplates obtained at different reaction temperatures. The simulated diffraction pattern from the JCPDS databases is plotted for comparison.

tions. An equilibrium structure is characterized by all real frequencies, whereas a transition state has one and only one imaginary frequency.

Results and Discussion

(A) Preparation of $Cu_{1.75}S$ Nanoplates: Reaction of CuTB−TOP with DDT. From earlier work in our laboratory, we have confirmed that neat CuTB precursor will decompose in a long-chain amine at room temperature to give Cu_2S nanoparticles.[27] In the present work, we noticed that slight warming to ~110 °C is required to decompose CuTB if amine is replaced with thiol. In particular, when CuTB dissolved in TOP is injected into hot DDT, uniform nanoplates were isolated. Figure 1 shows the representative XRD pattern of the nanoplates obtained at different reaction temperatures. All the diffraction peaks could be indexed to $Cu_{1.75}S$ (JCPDS 23-958) roxbyite phase, with their peak widths broadening as the reaction temperature increases. This indicates a decreasing crystallite size with temperature, in accordance with the Scherer equation.[28] From the XRD analysis, phase-pure $Cu_{1.75}S$ nanocrystals are obtained from this method.

From the TEM and SEM images shown in Figures 2 and 3, we can see that abundant $Cu_{1.75}S$ nanoplates are generated by this reaction. The nanoplates have a uniform hexagonal morphology and are fairly monodispersed, with an average hexagonal apex diameter of 62.1 ± 4.7 nm. The average thickness of the nanoplates is 15.5 nm, with a distribution of 7.9% (Figure 2a). The SAED pattern of the sample (Figure 2b) exhibits polycrystalline diffraction rings that can be indexed to the monoclinic structure of roxbyite $Cu_{1.75}S$. Clear lattice planes extending to the edges in the HRTEM images confirm the good crystallinity.

Images c and d of Figure 2 show two HRTEM images illustrating the two different orientations adopted by the nanoplates. In Figure 2c, a nanoplate is resting on its face, with the longer axis parallel to the substrate showing a lattice spacing of 3.0 Å. Figure 2d shows a nanoplate oriented perpendicular to the substrate with a lattice spacing of 3.4 Å. These monodispersed nanoplates either self-assemble by resting on their faces into hexagonally closed-packed (hcp) arrays, or stack together by lying perpendicular to the substrate into a long wormlike arrangement, as seen in Figure

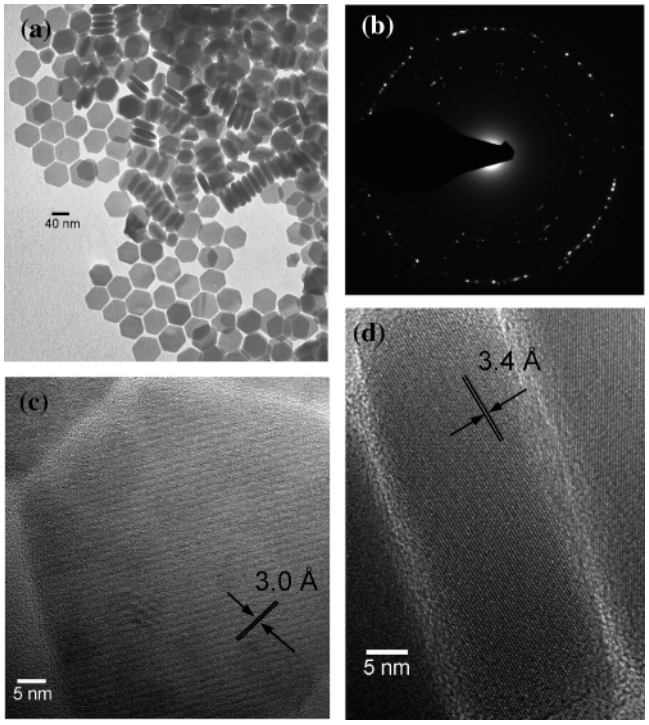

Figure 2. (a) Representative TEM image of the nanoplates produced at 135 °C, (b) SAED pattern of the nanocrystals, (c,d) HRTEM images of the top and side view of the nanoplates, respectively.

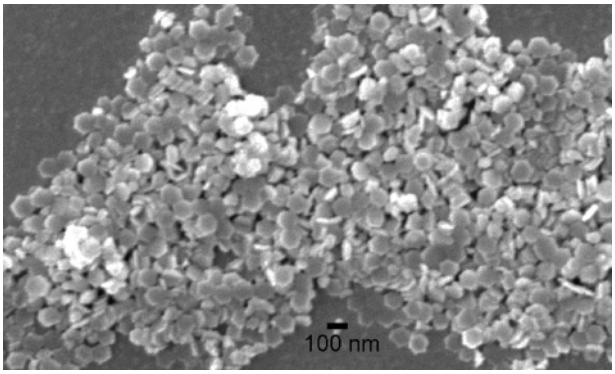

Figure 3. Representative SEM image of the nanoplates produced at 135 °C, showing clusters of the abundant nanoplates.

(26) Frisch, M. J.; Trucks, G. W.; Schlegel, H. B.; Scuseria, G. E.; Robb, M. A.; Cheeseman, J. R.; Zakrzewski, V. G.; Montgomery, J. A., Jr.; Stratmann, R. E.; Burant, J. C.; Dapprich, S.; Millam, J. M.; Daniels, A. D.; Kudin, K. N.; Strain, M. C.; Farkas, O.; Tomasi, J.; Barone, V.; Cossi, M.; Cammi, R.; Mennucci, B.; Pomelli, C.; Adamo, C.; Clifford, S.; Ochterski, J.; Petersson, G. A.; Ayala, P. Y.; Cui, Q.; Morokuma, K.; Malick, D. K.; Rabuck, A. D.; Raghavachari, K.; Foresman, J. B.; Cioslowski, J.; Ortiz, J. V.; Baboul, A. G.; Stefanov, B. B.; Liu, G.; Liashenko, A.; Piskorz, P.; Komaromi, I.; Gomperts, R.; Martin, R. L.; Fox, D. J.; Keith, T.; Al-Laham, M. A.; Peng, C. Y.; Nanayakkara, A.; Gonzalez, C.; Challacombe, M.; Gill, P. M. W.; Johnson, B.; Chen, W.; Wong, M. W.; Andres, J. L.; Gonzalez, C.; Head-Gordon, M.; Replogle, E. S.; Pople, J. A. *Gaussian 98*, revision A.7; Gaussian, Inc.: Pittsburgh, PA, 1998.
(27) Zhang, Z; Lim, W. P.; Wong, C. T.; Yin, F.; Chin, W. S. Submitted for publication.
(28) (a) Cullity, B. D. *Elements of X-ray Diffraction*, 2nd ed.; Addison-Wesley: Reading, MA, 1978. (b) Taylor, A. *X-ray Metallogaraphy*; Wiley: New York, 1961, 674.

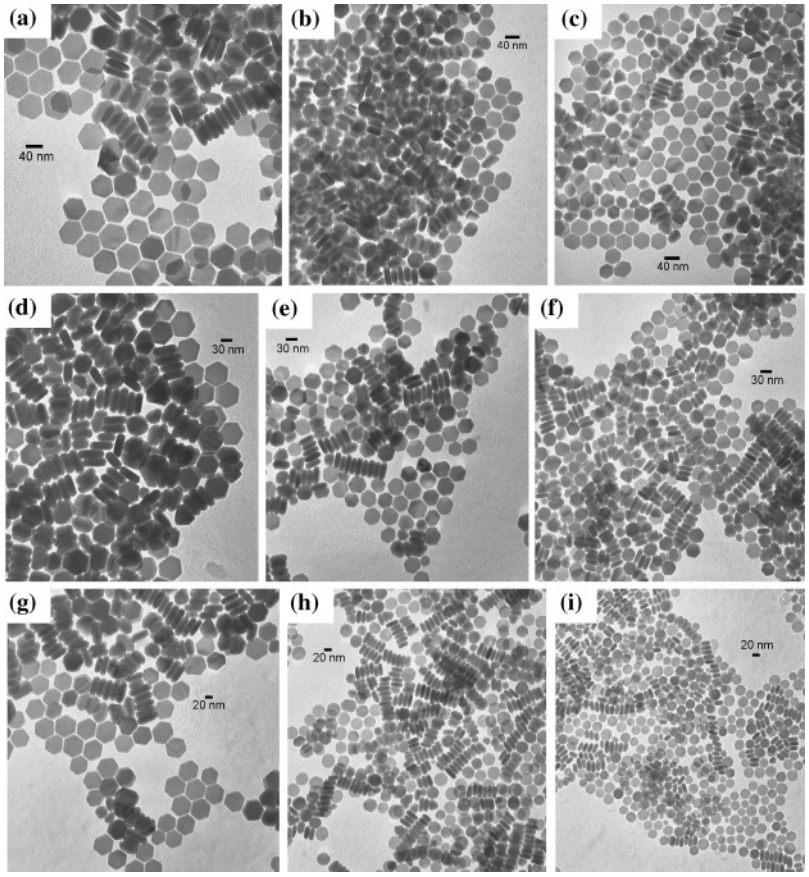

Figure 4. Representative TEM images of the nanoplates produced at (a−c) 135, (d−f) 160, and (g−i) 180 °C, with [DDT]/[CuTB] ratios of 30, 40, and 50, respectively.

2a. From our numerous microscopic observations, we have confirmed that nanoplates of different sizes exhibit similar lateral (∼2.6 nm in the hcp arrays) or vertical (∼1.4 nm between the stacked plates) interplate distances. Because the zigzag chain of DDT is estimated to be ∼15 Å in length, we suspect the adsorbed DDT molecules self-assemble rather uniformly onto the faces of the nanoplates, thus leading to strong interdigitation between their alkyl chains on adjacent nanoplates.

Although the formation of Cu_xS disks has been reported by Gao[16a] and Korgel[22] et al., the control of their size, shape, and the aspect ratio has not been reported. We will demonstrate in the following that the size and shape, as well as the aspect ratio (i.e., diameter/thickness), of the nanoplates can be tuned by the [DDT]/[CuTB] ratio and the reaction temperature. TEM images of $Cu_{1.75}S$ nanoplates synthesized at 135 °C (Figure 4a−c) and 160 °C (Figure 4d−f) show that the size of the plate decreases with an increase in DDT concentration. This is a trend consistent with the role of DDT as the capping agent. On the other hand, whereas hexagonal nanoplates are exclusively formed at temperatures below 160 °C, formation of circular nanoplates is observed at 180 °C and high DDT concentration. TEM images of the nanoplates synthesized at 180 °C reveal the shape variation from hexagonal (Figure 4g) to smaller circular nanoplates (Figures 4h,i) with increasing DDT concentration. At even higher reaction temperatures, mixtures of hexagonal and circular plates with large size distributions are always observed. The effect of DDT concentration and reaction temperature on the diameter, thickness, and aspect ratio of the prepared $Cu_{1.75}S$ nanoplates is summarized in Table 1.

Table 1. Summary of the Size and Shape of $Cu_{1.75}S$ Nanoplates Obtained under Various Reaction Conditions

[DDT]/[CuTB]	reaction T (°C)	diameter (nm)	thickness (nm)	aspect ratio	morphology
20	135	85.1 ± 8.5	19.3 ± 4.1	4.4	hexagonal
30	135	62.1 ± 4.7	15.5 ± 1.3	4.1	hexagonal
40	135	47.1 ± 4.2	15.2 ± 1.4	3.1	hexagonal
50	135	41.6 ± 4.1	15.2 ± 1.4	2.7	hexagonal
30	160	60.7 ± 5.4	17.8 ± 2.0	3.4	hexagonal
40	160	42.6 ± 4.0	14.4 ± 1.0	3.0	hexagonal
50	160	34.1 ± 3.6	13.0 ± 0.8	2.6	hexagonal
30	180	51.6 ± 4.9	15.6 ± 1.6	3.3	hexagonal
40	180	30.7 ± 2.9	10.6 ± 0.8	2.9	circular
50	180	23.0 ± 3.1	9.9 ± 0.8	2.3	circular
30	210	34.2 ± 19.2	12.8 ± 1.1	2.7	circular & hexagonal
40	210	33.0 ± 9.4	12.5 ± 1.3	2.6	circular & hexagonal
50	210	23.0 ± 8.6	11.7 ± 1.5	2.0	circular & hexagonal

The influence of temperature and [DDT]/[CuTB] ratio can be more clearly followed using correlation plots as shown in Figure 5. In general, both the diameter (Figure 5a) and thickness (Figure 5b) of the nanoplates decrease as the [DDT]/[CuTB] ratio increases. However, an exception was observed for samples prepared at 135 °C, where nanoplates with almost the same thickness are obtained at [DDT]/[CuTB] ratios from 30 to 50. When the percentage decrease in the plate diameter or thickness is plotted in Figure 5c, it is clear that changes in plate diameter are always much larger than those in the plate thickness. This leads to an overall decrease in the aspect ratio of the nanoplates with increasing DDT concentration, as shown in Figure 5d. Thus, we can

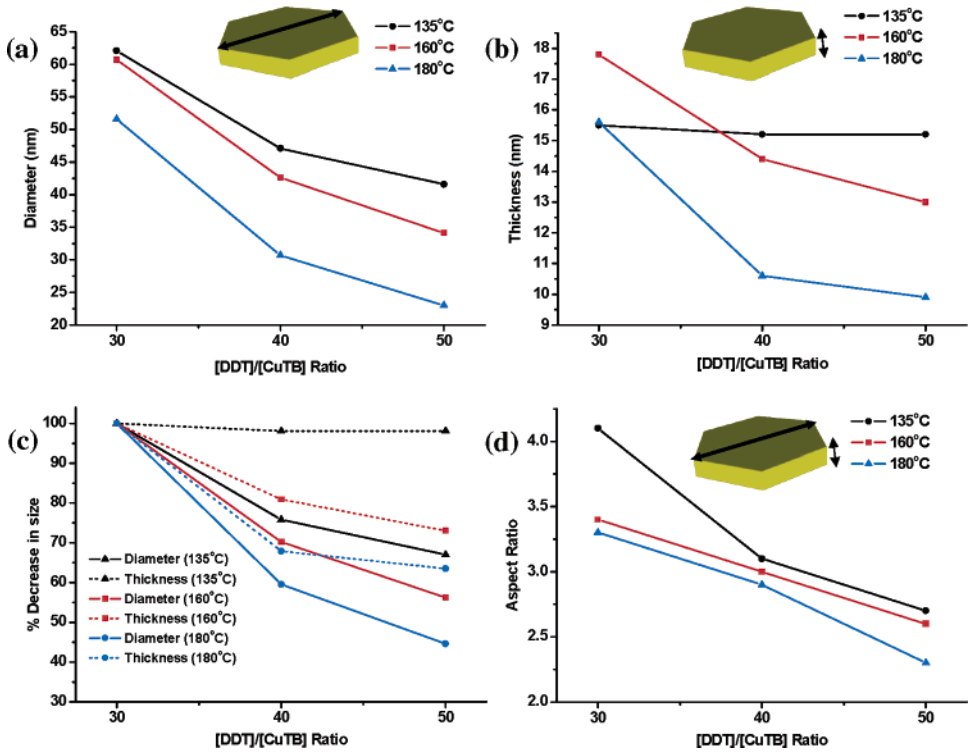

Figure 5. Effect of temperature and [DDT]/[CuTB] ratio on the (a) diameter, (b) thickness, (c) change in diameter and thickness, and (d) aspect ratio of the nanoplates.

conclude that the diameter of the nanoplates has a stronger dependence on the DDT concentration as compared to their thickness. This observation suggests a preferential capping on the faces of the nanoplates by DDT, inducing a higher sideways (i.e., 2D) growth rate of the nanocrystals.

The enforcement of such sideways 2D growth seems to be most successful when the reaction is carried out at 135 °C, such that the nanoplates have essentially ceased to grow in thickness within [DDT]/[CuTB] ratios between 30 and 50 (Figure 5b). Control experiments at [DDT]/[CuTB] = 20 at this temperature, however, show an abrupt increase in thickness to ~19 nm (Table 1). This suggests that, at a [DDT]/[CuTB] ratio below 30, the amount of DDT present becomes insufficient to effectively cover the top faces of the nanoplates to impede further growth in thickness. At temperatures higher than 135 °C, on the other hand, DDT molecules seem to have lost this preferential binding on the faces of the nanoplates. We also noted that smaller or more circular nanoplates are obtained as temperature increases, indicating a higher nucleation rate at such conditions.

(B) Preparation of Faceted Cu_2S Nanocrystals: Reaction of CuTB−TBPT with DDT. When TOP in our reaction mixture is replaced with TBPT, we observed that faceted nanocrystals are obtained exclusively in place of the above $Cu_{1.75}S$ roxbyite nanoplates. XRD patterns of the faceted nanocrystals reveal a pure hexagonal chalcocite Cu_2S phase, as shown in Figure 6. HRTEM images of the faceted nanocrystals (Figure 7) show sharp lattice fringes with 2.0 Å spacing, corresponding to the {110} planes of the nanocrystals.

We have also investigated the effect of temperature and [DDT]/[CuTB] ratio on the morphology and sizes of the prepared Cu_2S nanocrystals. TEM analysis of the products

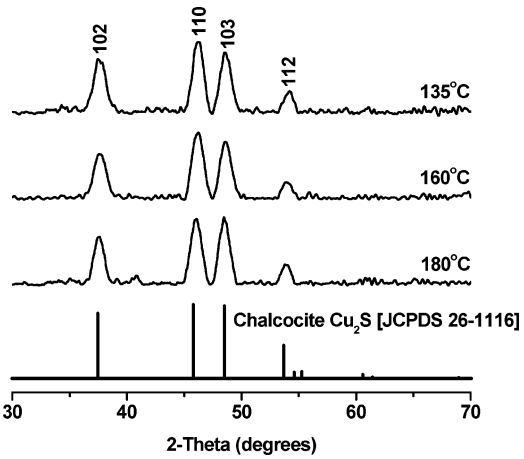

Figure 6. Representative XRD patterns of the faceted Cu_2S nanocrystals obtained at different reaction temperatures. The simulated diffraction pattern from the JCPDS databases is plotted for comparison.

indicated faceted morphology in all cases, with nanocrystals varying between ~5 and 9 nm in size. The average crystal sizes decrease similarly with increases in both temperature and DDT concentration (see the Supporting Information, S1).

(C) Activation and Stabilization Role of Reagents. In this and the following sections, we attempt to understand the role of reagents used (DDT, TOP, TBPT) in the size- and phase-control of the nanocrystals. In our method, nanocrystals are generated from the decomposition of CuTB precursor. Although we have found that CuTB can decompose in a long-chain amine at room temperature,[27] TGA of CuTB shows that the onset of decomposition occurs at temperatures above 200 °C (see the Supporting Information, S2). Thus, it was suggested that the amine is both the capping as well as the activating agent; a similar reaction mechanism

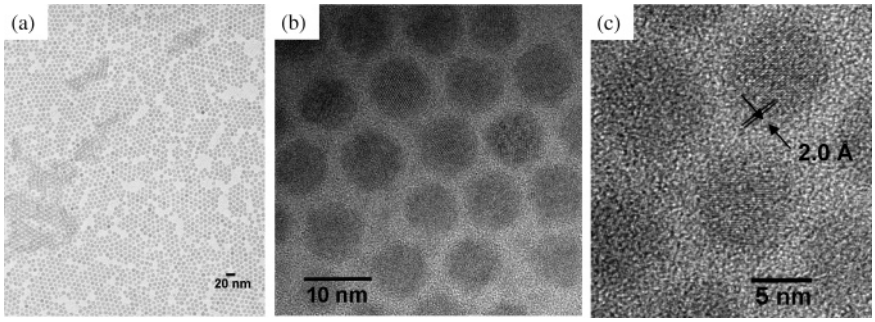

Figure 7. Representative (a) TEM and (b,c) HRTEM images of the nanocrystals produced from the reaction of CuTB−TBPT with DDT.

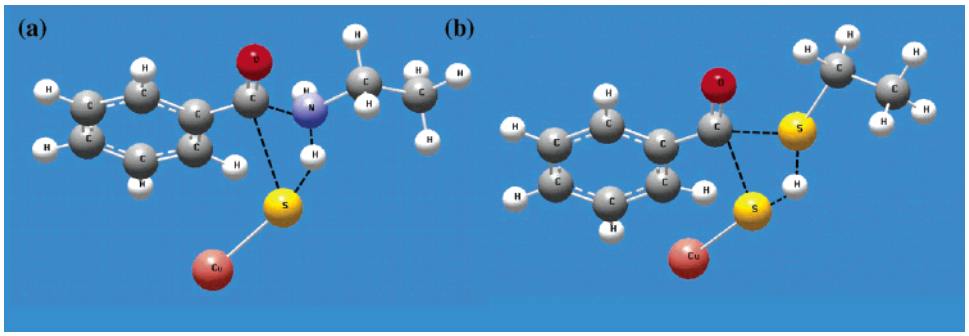

Figure 8. B3LYP/LanL2DZ optimized transition-state structures for the reaction of CuTB with (a) $C_2H_5NH_2$ and (b) C_2H_5SH.

Table 2. Important B3LYP/LanL2DZ Geometrical Parameters of the Transition-State (TS) Structures (refer to Figure 8) Compared with Those in CuTB, Ethylamine (EA), or Ethanethiol (ET)[a]

	Cu−S bond (Å)		C−S bond (Å)		C−N bond (Å)	N−H bond (Å)	
	CuTB	TS	CuTB	TS	TS	EA	TS
reaction between CuTB & EA	2.348	2.173	1.812	2.669	1.601	1.017	1.059
	Cu−S_p bond (Å)		C−S_p bond (Å)		C−S_t bond (Å)	S_t-H bond	
	CuTB	TS	CuTB	TS	TS	ET	TS
reaction between CuTB & ET	2.348	2.276	1.812	2.225	2.429	1.381	1.757

[a] S_p refers to the sulfur atom in CuTB; S_t refers to the sulfur atom in ET; C refers to the thiocarboxylate carbon atom in CuTB.

whereby the amine initiates a nucleophilic attack onto the electrophilic carbon atom of thiocarboxylate is proposed[1a,29]

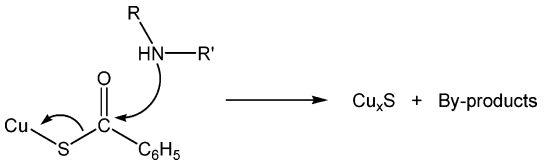

In the present work, heating to ∼110 °C is required to decompose CuTB with DDT, suggesting that thiol is a weaker activating agent compared to amine.

To confirm the proposed mechanism, DFT calculations were performed to model the nucleophilic attack of simpler ethylamine and ethanethiol molecules. Figure 8 and Table 2 give the optimized transition-state structures and their important geometrical parameters. Indeed, DFT optimization confirms the elongation of one C−S bond and the formation of a C−N or C−S bond, respectively, in the two transition states. The reaction is predicted to be exothermic, with energy barriers of 109.2 and 157.3 kJ/mol, respectively, for the amine- and thiol-mediated reactions. Although the calculation models are highly simplified, the located transition-state structures as well as the energy barriers predicted support our proposed mechanism and that thiol is a relatively weaker activating agent (∼50 kJ/mol higher in energy barrier) compared to amine for this reaction.

Although amine facilitates the decomposition of CuTB at room temperature, we have found that heating to ∼100 °C is required if CuTB is dissolved in TOP or TBPT prior to the addition of amine. Hence, TOP or TBPT in this case acts as a stabilizing agent for the reaction. It is commonly believed that coordination complexes are formed with these ligands and thus the decomposition of CuTB is impeded. To verify this, DFT calculations were also performed on CuTB coordinated with various number of PMe_3 and $P(OMe)_3$ ligands (i.e., simpler models for TOP and TBPT, respectively). The predicted energy values and the optimized structures of the complexes are given in S3 and S4 of the Supporting Information. In summary, DFT calculations predicted the formation of these complexes with increasing stability via coordination, up to a maximum of 3 ligands per complex in both cases. The stabilization energy is predicted to be slightly larger (∼40 kJ/mol) for the PMe_3 complexes compared to the $P(OMe)_3$ complexes. This is in line with the expectation that $P(OR)_3$ is a less-electron-donating ligand

(29) Zhang, Z. H.; Lee, S. H.; Vittal, J. J.; Chin, W. S. *J. Phys. Chem. B* **2006**, *110*, 6649.

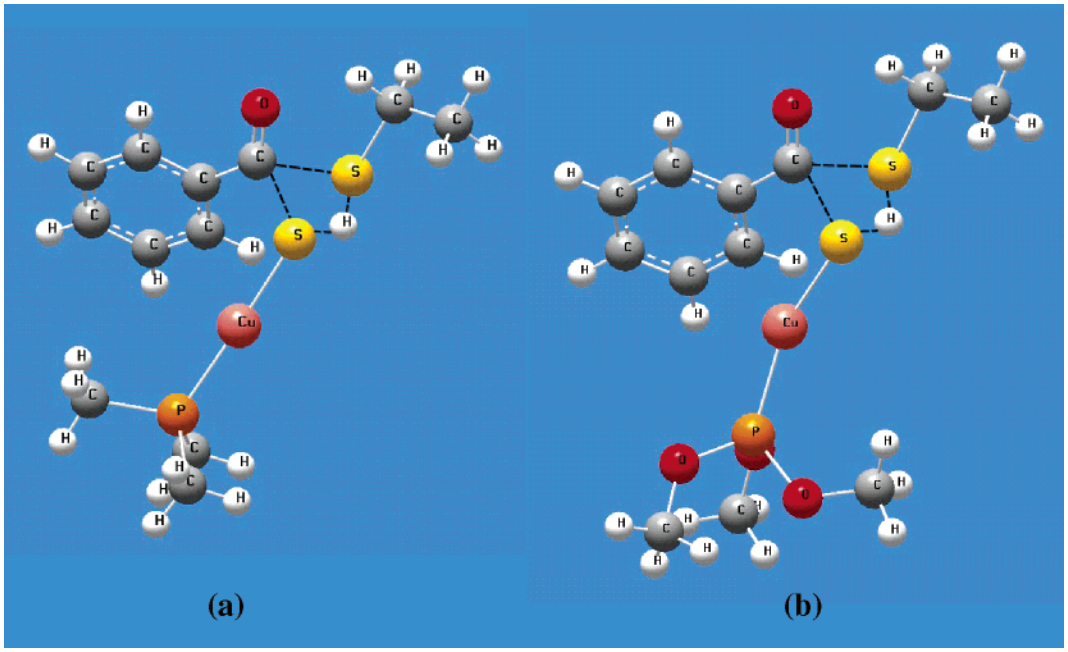

Figure 9. B3LYP/LanL2DZ optimized transition-state structures for the reaction between C_2H_5SH and (a) CuTB−PMe_3 and (b) CuTB−$P(OMe)_3$.

compared to PR_3 (R = alkyl). The calculated coordination P−Cu bond length ranges from 2.3−2.4 Å, increasing slightly with the number of ligands attached. It is known that the coordination bond is ~2.2 Å, similar to that for Cu−phosphine complexes.

Thus, on the basis of the above insights, we can optimize the kinetics of CuTB decomposition by varying the amount and nature of the activating (amine/thiol) as well as the stabilizing (TOP/TBPT) agents. In our preparation of nanoplates (section A), DDT was advantageously used as the activating agent, whereas TOP was used as the stabilizing agent. Thiol was chosen instead of amine because the decomposition of CuTB−TOP in amine was found to be too rapid, leading to uncontrollable nucleation and growth of polydispersed crystals (see the Supporting Information, S5). On the other hand, DDT allowed better control of the reaction; the sizes and shapes (circular or hexagonal plates) of the products can be readily optimized by varying the [DDT]/[CuTB] ratio and temperature, as shown in section A.

(D) Crystalline Phase Control of the Nanocrystals. It is most interesting in our study to find that nanocrystals of different crystal phases are generated when TOP was replaced with TBPT (section B). It has been reported that crystal phases of nanocrystals can be altered by temperature[30] or pressure-driven transformation.[31] Recently, Ghezelbash et al. described the synthesis of CuS and $Cu_{1.8}S$ nanocrystals by varying the Cu:S mole ratio.[32] In our case, however, the different phases of Cu_xS are produced from a molecular precursor under similar temperatures at ambient pressure. As control experiments, we thus carried out the reaction of CuTB in pure TOP and TBPT. In the absence of any activating agent (amine or thiol), decomposition was achieved only at temperatures above 200 °C; it was found that both products in this case were chalcocite Cu_2S phase (see the Supporting Information, S6).

Table 3. Summary of the Crystalline Phases of Cu_xS Nanocrystals Obtained under Various Reaction Conditions

activating agent[a]	stabilizing agent[a]	T (°C)	crystalline phase
none	TBPT	210	chalcocite Cu_2S
none	TOP	210	chalcocite Cu_2S
DDT	TBPT	135−180	chalcocite Cu_2S
DDT	TOP	135−200	roxbyite $Cu_{1.75}S$
OA	TBPT	160	roxbyite $Cu_{1.75}S$
OA	TOP	160	roxbyite $Cu_{1.75}S$
DDT & small amount of OA	TBPT	160	roxbyite $Cu_{1.75}S$

[a] TOP = Trioctylphosphine, TBPT = tributylphosphite, DDT = dodecanethiol, OA = octylamine.

In summary, the influence of reaction conditions on the crystalline phases of the product is given in Table 3. We noticed that, in the presence of a strong activating agent such as amine, roxbyite $Cu_{1.75}S$ is obtained from both CuTB−TBPT and CuTB−TOP precursor complexes. In the presence of a weak activating agent such as thiol, chalcocite Cu_2S is obtained from the decomposition of CuTB−TBPT (section B), whereas roxbyite $Cu_{1.75}S$ is obtained from CuTB−TOP (section A). Without an activating agent, only chalcocite Cu_2S phase is obtained.

The different crystalline phase produced, we believe, is associated with the decomposition routes of CuTB leading to seeds of two different phases at similar temperatures. We propose that CuTB can undergo at least two competing decomposition routes resulting in the formation of chalcocite (route 1) or roxbyite (route 2) copper sulfide. In the absence of any activating agent, route 1 was found to be favored regardless of the type of stabilizing agent used (TOP or TBPT). In the presence of strong activating agent (amine), on the other hand, route 2 is dominating. We thus believe that decomposition via route 1 may be a simple thermolysis process, whereas decomposition via route 2 involves the

(30) Yu, W. W.; Wang, Y. A.; Peng, X. *Chem. Mater.* **2003**, *15*, 4300.
(31) Morgan, B. J.; Madden, P. A. *Nano Lett.* **2004**, *4*, 1581.
(32) Ghezelbash, A.; Korgel, B. A. *Langmuir* **2005**, *21*, 9451.

Table 4. Important B3LYP/LanL2DZ Geometrical Parameters for the Transition-State (TS) Structures as Compared to the Precursor (P) and Ethanthiol (ET)[a]

precursor complex	Cu−S_p bond (Å)		C−S_p bond (Å)		C−S_t bond (Å)	S_t−H bond	
	P	TS	P	TS	TS	ET	TS
CuTB−PMe_3	2.312	2.245	1.816	2.196	2.464	1.381	1.806
CuTB−$POMe_3$	2.440	2.268	1.796	2.204	2.453	1.389	1.805

[a] S_p refers to the S atom on the precursor and S_t refers to the S atom on ethanethiol.

proposed nucleophilic attack of the activating agent, resulting in the cleavage of S−C bond.[1a,29]

When a weak activating agent such as DDT is used, the two routes become competitive, dependent on the type of stabilizing agent used. Because TBPT is predicted to form a relatively less stable coordination complex compared to TOP, it seems that the less-stable precursor complex will decompose via route 1 to give chalcocite Cu_2S. As a control experiment to enhance the route 2 competitive mechanism, we added a small amount of amine to the decomposition mixture of CuTB−TBPT in DDT. Indeed, roxbyite $Cu_{1.75}S$ nanocrystals were isolated instead (Table 3). This thus confirms that route 2 is favored over route 1 in the presence of a strong activating agent.

To gain more insight into the relative energetics for the route 2 reaction between DDT and the two precursor complexes CuTB−TOP and CuTB−TBPT, we model the reaction using simpler ethanethiols, CuTB−PMe_3 and CuTB−$P(OMe)_3$. Figure 9 and Table 4 show the located transition-state structures and their important geometrical parameters. The DFT-predicted energy barriers are 158.9 and 164.7 kJ/mol, respectively, for the decomposition of CuTB−PMe_3 and CuTB−$P(OMe)_3$. The slightly lower barrier (∼6 kJ/mol) predicted for the CuTB−PMe_3 complex supports our observations that CuTB−TOP undergoes route 2 more readily compared to CuTB−TBPT under similar conditions. Although these calculations are highly simplified in view of the complexity of reactions occurring in the solution state, these results do provide, on a relative basis, for competitive reaction pathways of the precursor to be selected and hence different crystal phases of the products to be generated.

Conclusion

We have described a simple strategy for preparing phase-selective copper sulfide nanocrystals. The successful isolation of phase-pure and monodispersed roxbyite $Cu_{1.75}S$ nanoplates and faceted chalcocite Cu_2S nanocrystals demonstrated possible crystal engineering by manipulating the reaction kinetics of molecular precursors. In essence, we may summarize the following general guidelines for producing good nanocrystals from such precursors: (i) activating agent selected should not be too strong so that the reaction can be appropriately controlled, (ii) stabilizing agent can be suitably used to slow down a reaction that normally proceeds at/below room temperature so that an added parameter (i.e., *T*) can be utilized for optimization, (iii) a balance between [activating agent] and [stabilizing agent] may allow competitive reaction pathways to be preferentially selected. On this final point, we hope to demonstrate that DFT calculations could be used to provide some insight to the various possible reaction pathways.

The physical properties of these phase-pure nanoplates and nanocrystals are currently under investigation to provide insight on the effect of anisotropy in quantum confinement properties. These low-dimensional nanocrystals should lead to interesting research on the rational tuning of their optical and electrical properties. The possibilities of assembling these nanoplates, e.g., for the use as sacrificial templates for patterning, are also being explored.

Supporting Information Available: Summary of size dependency, TGA data, coordination effects, predicted optimized structures, representative TEM and XRD images. This material is available free of charge via the Internet at http://pubs.acs.org.

CM061686I